

Article

CO₂ Sorbents Based on Spherical Carbon and Photoactive Metal Oxides: Insight into Adsorption Capacity, Selectivity and Regenerability

Iwona Pełech, Ewelina Kusiak-Nejman, Piotr Staciwa, Daniel Sibera, Joanna Kapica-Kozar, Agnieszka Wanag, Filip Latzke, Karolina Pawłowska, Adrianna Michalska, Urszula Narkiewicz et al.

Special Issue

Nanocomposites as a Promising Type of Photocatalyst

Edited by

Dr. Madalina Ciobanu and Dr. Gabriela Petcu



Article

CO₂ Sorbents Based on Spherical Carbon and Photoactive Metal Oxides: Insight into Adsorption Capacity, Selectivity and Regenerability

Iwona Pelech ¹, Ewelina Kusiak-Nejman ^{1,*}, Piotr Staciwa ¹, Daniel Sibera ^{1,2}, Joanna Kapica-Kozar ¹, Agnieszka Wanag ¹, Filip Latzke ¹, Karolina Pawłowska ¹, Adrianna Michalska ¹, Urszula Narkiewicz ¹ and Antoni W. Morawski ¹

¹ Department of Inorganic Chemical Technology and Environment Engineering, Faculty of Chemical Technology and Engineering, West Pomeranian University of Technology in Szczecin, Pułaskiego 10, 70-322 Szczecin, Poland

² Faculty of Civil and Environmental Engineering, West Pomeranian University of Technology in Szczecin, al. Piastów 50a, 70-311 Szczecin, Poland

* Correspondence: ekusiak@zut.edu.pl; Tel.: +48-91-449-4244

Abstract: This work aimed to obtain hybrid composites based on photoactive metal oxide and carbon having adsorption properties. The materials, composed of titanium dioxide or zinc oxide and spherical carbon, were obtained from resorcinol-formaldehyde resin, treated in a solvothermal reactor heated with microwaves and then subjected to carbonization, were received. The functional groups of pure carbon spheres (unsaturated stretching C=C, stretching C–OH and C–H bending vibrations), CS/ZnO and CS/TiO₂ samples were determined by FT-IR analysis. The characteristic bands for ZnO and TiO₂ were observed below 1000 cm⁻¹. The thermal oxidative properties are similar for TiO₂- and ZnO-modified carbon spheres. We have observed that the increased carbon sphere content in nanocomposites results in starting the decomposition process at a lower temperature, therefore, nanocomposites have a broader combustion temperature range. The effect of the oxides' addition to carbon spheres on their adsorption properties was evaluated in detail by examining CO₂ adsorption from the gas phase. The selectivity of CO₂ over N₂ at a temperature of 25 °C and pressure of 1 bar (a novelty in testing CS-based sorbents) calculated for 3.00 CS/TiO₂ and 4.00 CS/ZnO was 15.09 and 16.95, respectively. These nanocomposites exhibit excellent cyclic stability checked over 10 consecutive adsorption–desorption cycles.

Keywords: carbon spheres; titanium dioxide; zinc oxide; physical adsorption; carbon dioxide; CO₂/N₂ selectivity



Citation: Pelech, I.; Kusiak-Nejman, E.; Staciwa, P.; Sibera, D.; Kapica-Kozar, J.; Wanag, A.; Latzke, F.; Pawłowska, K.; Michalska, A.; Narkiewicz, U.; et al. CO₂ Sorbents Based on Spherical Carbon and Photoactive Metal Oxides: Insight into Adsorption Capacity, Selectivity and Regenerability. *Molecules* **2022**, *27*, 6802. <https://doi.org/10.3390/molecules27206802>

Academic Editors: Madalina Ciobanu and Gabriela Petcu

Received: 13 September 2022

Accepted: 5 October 2022

Published: 11 October 2022

Publisher's Note: MDPI stays neutral with regard to jurisdictional claims in published maps and institutional affiliations.



Copyright: © 2022 by the authors. Licensee MDPI, Basel, Switzerland. This article is an open access article distributed under the terms and conditions of the Creative Commons Attribution (CC BY) license (<https://creativecommons.org/licenses/by/4.0/>).

1. Introduction

It is an undeniable fact, supported by the global scientific consensus, that increasing anthropogenic global greenhouse gas emissions leads to irreversible changes in the Earth's climate. A limit has been set to prevent this: an increase in the global average temperature of less than 1.5 °C relative to pre-industrial times. For this to be possible, all sources of CO₂ emissions must be decarbonized by 2050 [1]. The energy and heating sector is responsible for the largest share of global greenhouse gas emissions [2], most of which is carbon dioxide. Therefore, as long as fossil fuels remain the main energy source in the world, it will not be possible to achieve this goal. In order to reduce the concentration of CO₂ in the atmosphere, it is necessary to switch to obtaining energy from renewable sources such as wind, solar or geothermal. However, nuclear power should be the basis due to one of the lowest carbon footprint values, averaging 66 g CO₂/kWh, and its independence from weather conditions [3]. At the same time, it is necessary to introduce technologies to eliminate carbon dioxide from the exhaust gases of already existing emission sources.

Currently, research is being conducted, and technologies are being implemented in two directions: carbon capture and storage (CCS), and carbon capture and utilization (CCU) [4,5]. Separated CO₂ can be stored in several ways. One of these is the mineralization of carbon dioxide into calcite, magnesite, dolomite or various forms of magnesium hydrocarbonates [6]. It can also be stored in depleted oil or gas fields and adsorbed into coal seams [7]. The second method involves the conversion of carbon dioxide into valuable products such as fuels, fertilizers or substrates for synthesis [8]. However, for CO₂ to be stored or used, it must first be captured from the flue gas stream. Many technologies are dedicated to CO₂ capture: absorption, adsorption, membrane separation, calcium looping, cryogenic and chemical looping [9,10]. However, despite intensive research and promising results, most of these technologies are not ready for industrial application in carbon dioxide capture or they are highly energy demanding.

The advantages of adsorption over other CO₂ capture technologies are high adsorption capacity, regenerability, ease of operation of adsorption plants and material stability. Many materials have been tested as potential CO₂ sorbents: MOFs, zeolites, metal oxides, mesoporous silicas or porous carbon materials [9]. Carbon-derived materials include nanotubes, nanowires, graphene and graphene oxides, and activated carbons or carbon spheres [11,12]. There are several parameters that a promising sorbent must fulfill: low manufacturing cost, high selectivity towards the adsorbed component, high sorption capacity, ease of regeneration and mechanical and thermal durability. Carbon spheres (CS) are materials that meet most of these criteria. They can be obtained in several ways: hydrothermally, arc discharge, chemical vapor deposition (CVD) or ultrasound treatment [13–16]. However, the most popular and most straightforward method to obtain them is the Stöber method, which was first used by Liu et al. [17]. In this process, the carbon source is a phenol-formaldehyde resin. Using this method, Wickaramantne and Jaroniec obtained carbon spheres with specific surface areas ranging from 390 to 669 m²/g (depending on the carbonization temperature). The sorption capacity of these materials was in the range of 1.4 to 3.02 mmol/g (from 3.6×10^{-6} to 4.5×10^{-6} mol/m²) [18]. To increase the efficiency of the adsorption process by carbon spheres, an activation process is necessary. This can be completed chemically or physically. Chemical activation can occur by treating the carbon spheres with compounds such as potassium hydroxide, potassium carbonate, potassium oxalate or zinc chloride [19–22]. Physical activation occurs by exposing the spheres to steam or carbon dioxide at the carbonization step [23,24]. Chemical activation significantly increases the specific surface area and the sorption capacity towards carbon dioxide at 0 and 25 °C. For example, in the work of Jaroniec et al., activation of spheres with potassium oxalate resulted in a specific surface area of 2130 m²/g, and carbon dioxide sorption capacity equals 6.6 mmol/g (3.09×10^{-6} mol/m²) [25]. The addition of a microwave excitation step made it possible to obtain spheres with an area of up to 1648 m²/g and CO₂ sorption capacities ranging from 3.86 to 5.03 mmol/g at 25 °C (from 3.05×10^{-6} to 3.27×10^{-6} mol/m²) [26].

Carbon materials are known for their ability to improve the photocatalysis process, mainly due to the increased dispersion of the photocatalyst because of the high specific surface area of these materials. Moreover, their high electrical conductivity regulates the photocatalytic activity in the visible light range and attracts photogenerated electrons from the photocatalyst surface [27]. Therefore, carbon spheres modified with such photocatalysts as titanium dioxide or zinc oxide may be future materials capable of efficiently adsorbing and transforming CO₂ into valuable compounds. In both cases, first attempts have already been made to obtain such composites. Zinc oxide-modified carbon spheres were first obtained in 2002 from an ion-exchangeable resin with the addition of a complex $[\text{Zn}(\text{NH}_3)_2]^{2+}$. As a result, materials with a specific surface area ranging from 201 to 523 m²/g were obtained, in which a decrease in specific surface area with increasing ZnO content was noted [28]. ZnO/CS hybrid materials were obtained by Wang et al. in 2007 [29] using a surface-coating method. The low specific surface area of these materials (6–18 m²/g) resulted from the complete surface-coating of the carbon spheres with zinc oxide, forming

various types of structures on them (e.g. described by the authors as “dandelions”). These composites showed high photocatalytic activity despite the low, specific surface area. In our previous studies, we investigated the effect of modification of carbon spheres with zinc oxide (obtained from ZnCl_2 or $\text{Zn}(\text{NO}_3)_2$), and activation with potassium oxalate, on their surface parameters and the sorption capacity towards carbon dioxide. The specific surface area of the obtained materials ranged from 381 to 1233 m^2/g , and the sorption capacity towards CO_2 in the best case reached 2.69 mmol/g (2.18×10^{-6} mol/ m^2) at 40 °C [30,31]. For the modification of CS with titanium dioxide, Wang et al. [32] obtained spheres using a template hydrothermal method, which resulted in materials with a specific surface area of 386 m^2/g , with 4.5 times higher photocatalytic activity than pure TiO_2 (Degussa P25). The N-doped melamine-formaldehyde spheres supporting anatase TiO_2 , synthesized by a two-step solvothermal method obtained by Bi et al. [33], showed a surface area in the range of 70 to 106 m^2/g , depending on the temperature of the hydrothermal treatment. Morawski et al. [34] obtained titanium dioxide-modified carbon spheres by microwave-assisted solvothermal synthesis using phenol-formaldehyde resin as the carbon source. The resulting material showed a sorption capacity towards CO_2 of 3.94 mmol/g (9.12×10^{-6} mol/ m^2) (at 40 °C) and a specific surface area of 432 m^2/g . For both the TiO_2 and ZnO-modified CS, the presence of metal oxides on the carbon spheres’ surface reduces the composite materials’ total surface area and sorption capacity. However, this can be compensated for by the chemical activation process of the carbon spheres.

For this paper, we wanted to determine the role of the addition of selected metal oxides (ZnO and TiO_2 in this particular case) in the adsorption removal of CO_2 on modified carbon spheres. Additionally, to our knowledge, the CO_2/N_2 selectivity measurements performed and described in this paper are presented for the first time for spherical carbon materials modified with metal oxides. This study advances the general knowledge of CO_2 physical adsorption utilizing carbon sphere-based composites.

2. Results and Discussion

The nanomaterials were subjected to FT-IR analysis to detect the various characteristic functional groups associated with the synthesized samples (spectra presented in Figure 1a,b). Both the CS/ TiO_2 and CS/ ZnO groups of samples and reference samples (bare TiO_2 , ZnO and CS) are characterized by very similar FT-IR spectra. A broad band with a maximum at 3429 cm^{-1} is indexed to the bending and stretching modes of hydroxyl groups present on the surface of tested nanomaterials [35]. Considering that the bands with a maximum at 2924 and 2854 cm^{-1} are observed for all tested samples, they most likely correspond to the stretching vibration of hydroxyl compounds [36] related to the presence of KBr in a pellet. It is commonly known that KBr, due to its hygroscopic nature, can easily absorb water while preparing pellets. Other researchers also observed these peaks in KBr spectra [37]. However, in the case of materials with carbon spheres, these peaks can also be related to the C–H symmetric and asymmetric stretching vibrations, respectively, from the decomposition of ethyl alcohol used during the synthesis process to dissolve resorcinol, as described by Wang et al. [22] and Deshmukh et al. [38]. A similar observation was found for the peak at 1630 cm^{-1} , which can be both assigned to the O–H bonding vibration proving the water adsorption [39] and the Zn–OH bending vibration in the case of ZnO samples [40], as well as the unsaturated C=C stretching vibrations, indicating that a carbonization process occurred during the formation of the spheres [41]. Peaks between 1360–1490 cm^{-1} correspond to the C–H bending vibrations [42]. The existing peaks at 960–1300 cm^{-1} are assigned to C–OH stretching and –OH bending vibrations [43]. The presence of –OH groups is related to many residual hydroxyl groups forming the hydrophilic surface. The characteristic peaks of TiO_2 and ZnO are present below 1000 cm^{-1} . The prominent peak of TiO_2 is located in the 400–900 cm^{-1} range and corresponds to Ti–O stretching and Ti–O–Ti bridging stretching modes, while the characteristic band of ZnO is located in the range of 500 and 400 cm^{-1} and corresponds to the stretching mode of the Zn–O bond [44–46]. It is possible to observe different intensities of these peaks from the

same group of samples. It does not mean that the amount of TiO₂ or ZnO increases. The amount is the same for all composite nanomaterials, and this phenomenon is related to the CS amount—the peak intensity increases with decreases in the CS amount. With the higher amount of CS, the samples are darker and the measurement of the FT-IR spectra is more complicated.

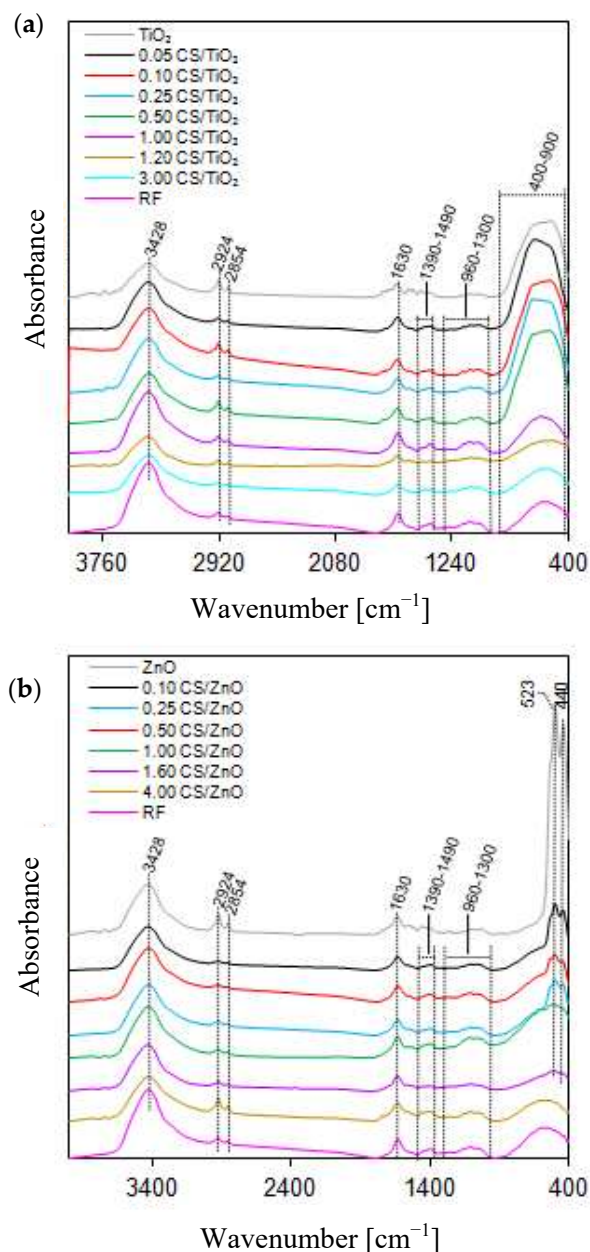


Figure 1. FT-IR spectrum of (a) CS/TiO₂ and (b) CS/ZnO samples.

The TG/DTG curves of the thermal oxidative stability of all the TiO₂- or ZnO-modified samples with different carbon sphere contents are shown in Figure 2a,b and Figure 3a,b, respectively. In the case of reference TiO₂ and ZnO semiconductors, only 2.30 and 1.25% weight losses were observed in a temperature range of 40–290 °C. That weight loss was attributed to the desorption of the physically adsorbed water [47]. For the unmodified carbon sphere sample (assigned as CS), the total weight loss of about 99.6% was observed between 369 and 730 °C, corresponding to the differential thermogravimetric (DTG) profile with a maximum at 674 °C, which could be assigned to breaking C–O bonds and desorption of residual organic compounds [48]. The results also show that both groups of samples

have similar thermal behavior during the heat treatment, which means that TiO_2 or ZnO photocatalysts are characterized by high thermal oxidative stability. For all samples, the first typical, however negligible, step of weight loss is observable between 100 and 220 °C, corresponding to the DTG profile with a maximum at 160 °C, which can be mainly ascribed to the desorption of moisture and other gases physically adsorbed on the surface of samples [49,50]. The next step occurred within the temperature range of 220 °C until 370 °C reaching the maximum at 270 °C (on DTG curves) due to the thermal decomposition of amorphous carbon [51].

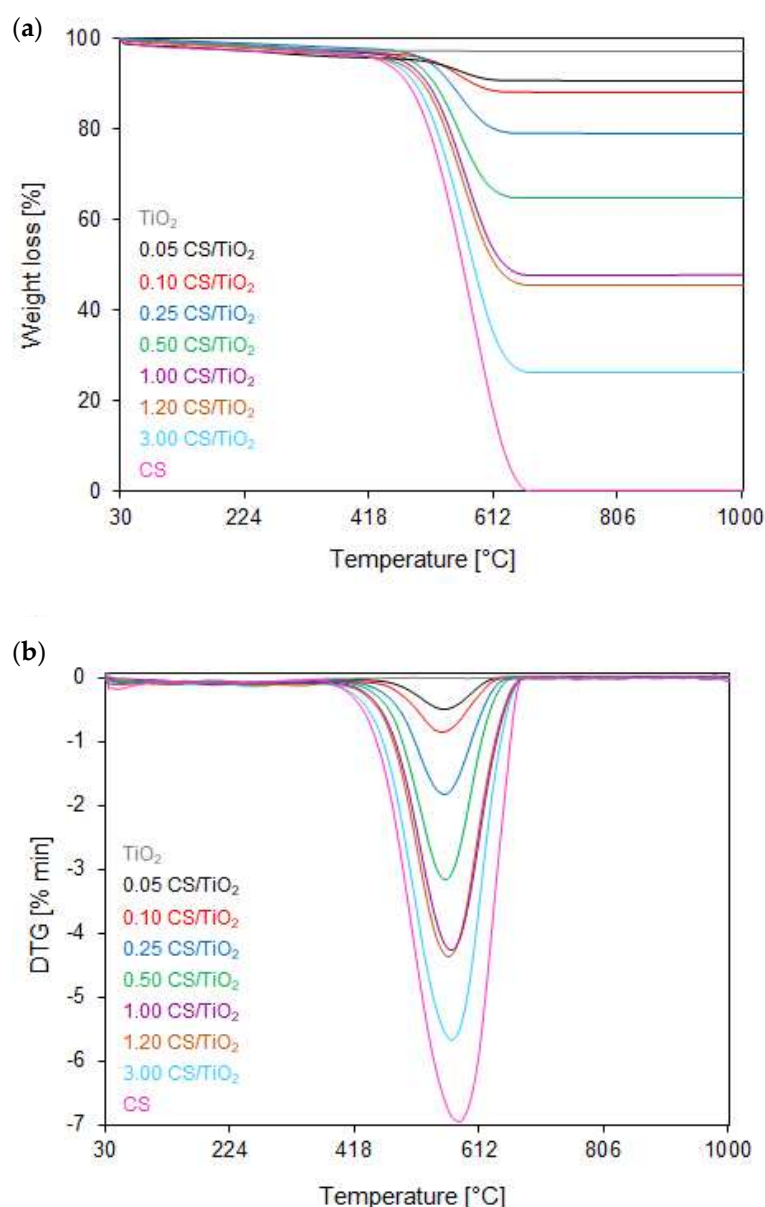


Figure 2. (a) TG and (b) DTG curves of reference TiO_2 , unmodified CS, and TiO_2 -modified nanocomposites with different carbon sphere contents measured in an oxidizing atmosphere.

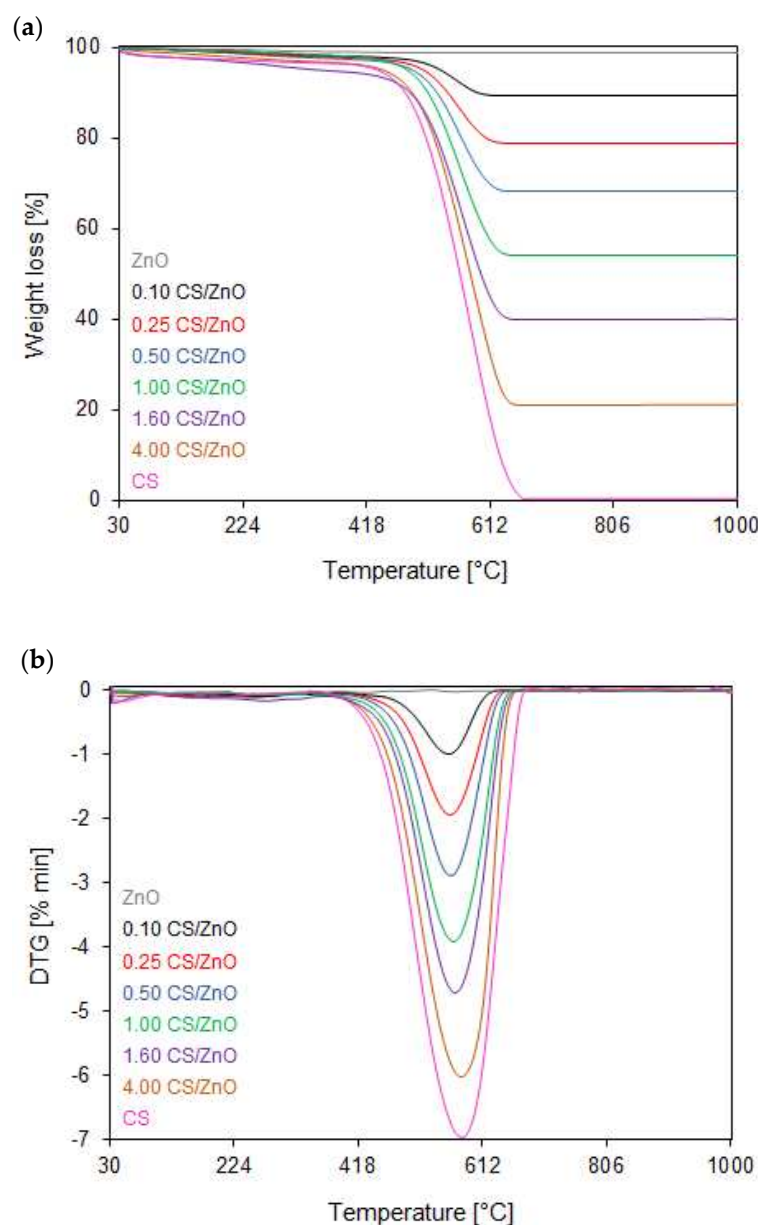


Figure 3. (a) TG and (b) DTG curves of reference ZnO, unmodified CS, and ZnO-modified nanocomposites with different carbon sphere contents measured in an oxidizing atmosphere.

It can be generally concluded that the thermal oxidative properties are broadly similar for TiO₂- and ZnO-modified carbon spheres. The increased carbon sphere content in nanocomposites results in starting the decomposition process at a slightly lower temperature, and therefore, they have a broader combustion temperature range (from 410 to 650 °C for TiO₂- and ZnO-modified carbon spheres with the lowest content carbon sphere and from 370 to 670 °C for TiO₂- and ZnO-modified carbon spheres with the highest CS content). This shows that the addition of CS inhibits the pyrolysis of TiO₂- and ZnO-modified composites. The total weight loss for the nanocomposites modified both with TiO₂ or ZnO, containing the lowest carbon content of 0.50 CS, exhibits from 8 to 33% within the temperature range of 380–666 °C and 410–660 °C, respectively, corresponding to the DTG profiles centered at ca. 560 °C. With the increased carbon spheres' content in nanocomposites, the total weight loss increased from 50 to 74 and 79%, and the maximum rate decomposition (DTG profile) shifted towards higher values, reaching the maximum at ca. 570 °C for the 1.20 CS/TiO₂ and 1.60 CS/ZnO, and 580 °C for 3.00 CS/TiO₂ and 4.00 CS/ZnO. This fact can be explained as follows: the higher the carbon and the lower

the oxygen contents, the more oxygen during combustion is required, thus, the combustion was delayed, contributing to a higher DTG value.

Based on the low-temperature ($-196\text{ }^{\circ}\text{C}$) nitrogen adsorption isotherms of the composites CS/TiO₂ (Figure 4) and CS/ZnO (Figure 5), the values of the specific surface area (S_{BET}), total pore volume (TPV), the volume of micropores ($V_{\text{m}} < 2\text{ nm}$), and volume of mesopores (V_{meso}) were determined and listed in Table 1. For all the obtained samples together with the increase in carbon content, the calculated values of the specific surface area are also growing. The lowest values of S_{BET} were received for 0.05 CS/TiO₂ and 0.05 CS/ZnO composites and amounted to 77 and 44 m^2/g , respectively. The specific surface area of the composites based on titanium dioxide is slightly higher than that of composites based on zinc oxide. However, it was observed only for the materials with carbon content up to 1 g, probably due to the higher specific surface area of pure titanium dioxide. Above that value, the values of S_{BET} were similar for both types of composites. The highest S_{BET} were obtained for 3.00 CS/TiO₂ and 4.00 CS/ZnO and amounted to 353 and 366 m^2/g , respectively.

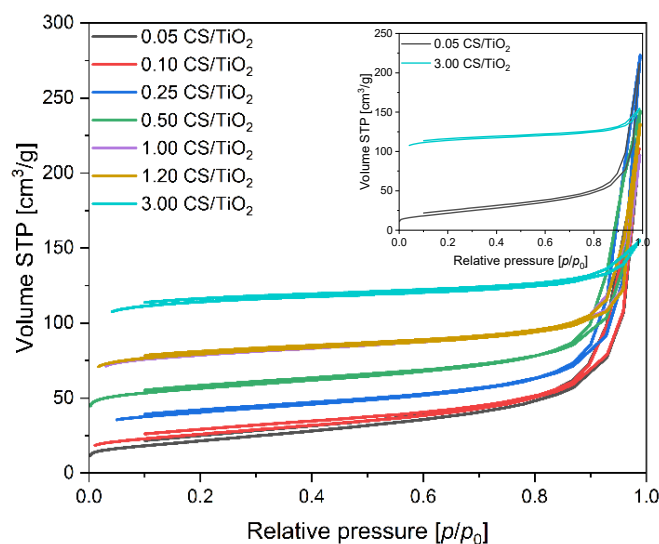


Figure 4. Nitrogen adsorption–desorption isotherms of all tested CS/TiO₂ composites, and selected 0.05 and 3.00 CS/TiO₂ samples (inset).

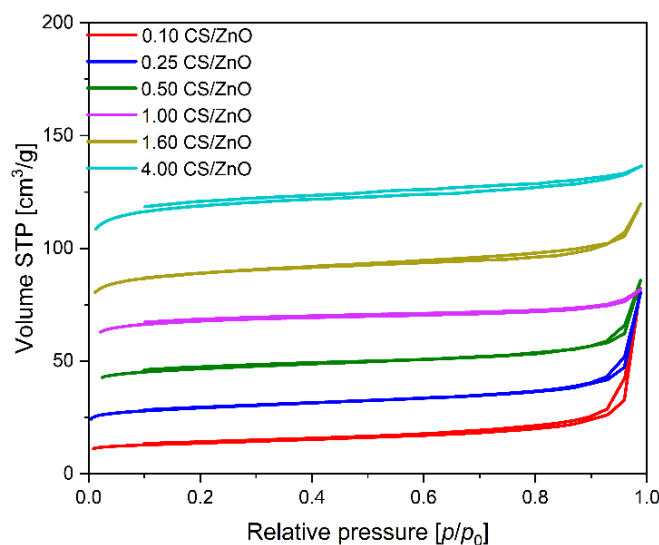


Figure 5. Nitrogen adsorption–desorption isotherms of CS/ZnO composites.

Table 1. Textural parameters and CO₂ sorption capacities for the activated carbon spheres.

Structural Properties → Sample Code ↓	S _{BET} (m ² /g)	TPV (cm ³ /g)	V _s (<1 nm) (cm ³ /g)	V _m (<2 nm) (cm ³ /g)	V _{meso} (cm ³ /g)	CO ₂ 0 °C (mmol/g)	CO ₂ 25 °C (mmol/g)
CS	455	0.26	0.19	0.22	0.04	3.25	2.43
TiO ₂	54	0.40	-	0.02	0.38	-	-
ZnO	11	0.03	-	0.00	0.03	-	-
0.05 CS/TiO ₂	77	0.33	0.02	0.02	0.31	0.41	0.29
0.10 CS/TiO ₂	89	0.34	0.03	0.03	0.31	0.42	0.33
0.25 CS/TiO ₂	132	0.43	0.04	0.04	0.39	0.79	0.54
0.50 CS/TiO ₂	181	0.37	0.07	0.07	0.30	1.33	0.90
1.00 CS/TiO ₂	247	0.33	0.10	0.11	0.22	1.75	1.22
1.20 CS/TiO ₂	248	0.36	0.11	0.11	0.25	1.91	1.36
3.00 CS/TiO ₂	353	0.24	0.13	0.16	0.08	2.45	1.66
0.10 CS/ZnO	44	0.13	0.02	0.02	0.11	0.31	0.21
0.25 CS/ZnO	92	0.13	0.04	0.04	0.09	0.68	0.46
0.50 CS/ZnO	145	0.13	0.06	0.06	0.07	1.12	0.74
1.00 CS/ZnO	209	0.13	0.09	0.10	0.03	1.54	1.11
1.60 CS/ZnO	275	0.18	0.11	0.12	0.06	2.08	1.41
4.00 CS/ZnO	366	0.21	0.15	0.17	0.04	2.70	1.88

S_{BET}—specific surface area; TPV—total pore volume; V_s—the volume of ultra-micropores with a diameter smaller than 1 nm; V_m—the volume of micropores with a diameter smaller than 2 nm; V_{meso}—the volume of mesopores with a diameter from 2 to 50 nm.

Significant differences for both series of materials were observed in the case of the total pore volume. For the samples based on titanium dioxide with the addition of 0.05 g of carbon spheres, TPV equaled 0.33 cm³/g. Similar values were also obtained for the composites with higher carbon content and, e.g. for the 1.20 CS/TiO₂ material, the calculated value of TPV was 0.36 cm³/g. Contrary to the samples mentioned above, an increase in carbon content of up to 3 g resulted in a reduction in the total pore volume value, and the 3.00 CS/TiO₂ TPV sample amounted only to 0.24 cm³. The samples based on zinc oxide and carbon spheres showed utterly different properties. The composites with carbon content ranging from 0.1 g to 1 g characterized the same TPV equaled 0.13 cm³/g, and these values were significantly lower than CS/TiO₂ composites. Together with the increase in carbon content of up to 1.6 and 4.0 g, TPV values were higher and amounted to 0.18 and 0.21 cm³/g for 1.60 CS/ZnO and 4.00 CS/ZnO, respectively. The total pore volume for CS/TiO₂ composites decreased, up to the value of 0.24 cm³/g (practically the same as for the pure carbon spheres), due to the low content of TiO₂, characterized by V_{meso} equal to 0.38 cm³/g. Pure zinc oxide has far fewer mesopores, only 0.03 cm³/g. Therefore, lower TPV values were noticed compared to CS/TiO₂ composites. For the sample 4.00 CS/ZnO, the total pore volume increased because the content of ZnO was low per 1 g of material, and TPV comes practically from the carbon.

According to IUPAC physisorption isotherm classification [52], CS/TiO₂ composites, except the sample containing 3.00 g of carbon, exhibited a type II physisorption isotherm, which is characteristic for mesoporous or non-porous materials with lower N₂ adsorption due to their much smaller BET surface area. In our case, the presence of carbon and titanium dioxide in the composites is responsible for the course of the isotherms. For pure TiO₂, a significant volume of mesopores is characteristic. Then, it can be concluded that the shape of the isotherm is derived from the mesoporous character of the composites. In all the samples, H3-type hysteresis loops were observed, and their presence implies the occurrence of mesoporous or plate-like particles with slit-shaped pores [53,54]. Hysteresis loops disappear with the increased mesopores (as seen in Figure 4, inset). The isotherm obtained for 3.00 CS/TiO₂ with the highest carbon contribution was of the mixed type I and II, indicating a high micropores' content. The calculated value confirms these observations, and according to the data presented in Table 1, the volume of micropores with a diameter smaller than 2 nm increased together with the carbon content in the samples from

0.02 cm³/g to 0.16 cm³/g for the 0.05 CS/TiO₂ and 3.00 CS/TiO₂ sample. Simultaneously, the differences between the composites were noted in the case of the volume of mesopores with diameters from 2 to 50 nm. For the CS/TiO₂ composites with the lowest carbon content, V_{meso} equaled 0.31 cm³/g, but for the sample with the addition of 1.2 g of carbon, it amounted to 0.25 cm³/g. A significant decrease in the mesopores content was recorded for the sample 3.00 CS/TiO₂, for which the volume of macropores equaled only 0.08 cm³/g.

For the composites consisting of carbon spheres and zinc oxide, the obtained nitrogen isotherms were a mixture of type I and II, characteristic of micro- and macroporous materials [31]. In the samples with a low content of carbon spheres, we can observe a hysteresis loop type H3, which disappeared in the samples with a large amount of carbon spheres, from 1 to 4 g. For 1.00 CS/ZnO, 1.60 CS/ZnO, and 4.00 CS/ZnO samples, the nitrogen adsorption isotherms have the shape typical of microporous materials. According to the data presented in Table 1, the volume of micropores with a diameter smaller than 2 nm increased together with the carbon content in the samples, such as in the case of the CS/TiO₂ samples, from 0.02 to 0.17 cm³/g for 0.10 CS/ZnO and 4.00 CS/ZnO sample, respectively. The opposite trend was observed in the case of the mesopores volume, such as in the case of the CS/TiO₂ composites. However, the values were much lower and were in the range of 0.11 cm³/g for 0.10 CS/ZnO and 0.04 cm³/g for 4.00 CS/ZnO.

The adsorption properties of the obtained materials were evaluated in detail by examining the CO₂ adsorption from the gas phase. The values of CO₂ adsorption at 0 and 25 °C calculated based on the isotherms presented in Figure 6 (for CS/TiO₂ composites) and Figure 7 (for CS/ZnO composites) are given in Table 1.

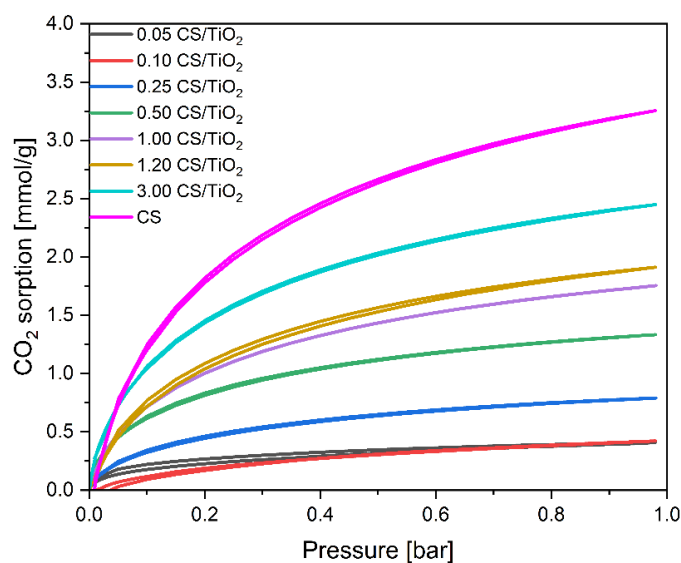


Figure 6. CO₂ sorption isotherms of the unmodified CS and obtained CS/TiO₂ composites.

Due to the similar distribution of pores, the course of the isotherms obtained for the CS/TiO₂ samples with the lowest carbon content (0.05 g and 0.1 g) was very similar. Increasing the carbon content up to 0.25 g resulted in the development of the surface area and mesoporosity of the composites, but the micropores' content changed only slightly. As the contribution of carbon in the samples further increased, higher values of the adsorbed CO₂ were detected. Similarly, the mesopores' volume decreased for the 1.00 CS/TiO₂ and 1.20 CS/TiO₂ samples with a carbon content of 1 and 1.2 g (1.75 and 1.91 mmol/g of CO₂ was adsorbed using these materials, respectively). The maximum amount of the adsorbed CO₂ was reached for the sample with the lowest mesopores' volume and equaled 2.45 mmol/g for the 3.00 CS/TiO₂ material.

The cyclic adsorption–desorption behavior was carried out for samples modified with TiO₂ or ZnO that achieved the highest CO₂ sorption capacity at both 0 and 25 °C among all the tested materials in this study (3.00 CS/TiO₂ and 4.00 CS/ZnO). The calculated

CO₂ capacities during ten consecutive adsorption–desorption cycles at 30 °C are shown in Figure 8.

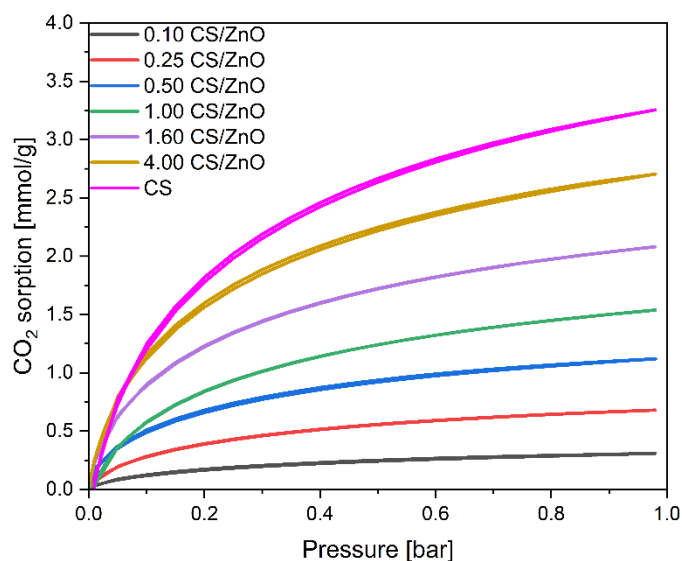


Figure 7. CO₂ sorption isotherms of the reference CS and the obtained CS/ZnO composites.

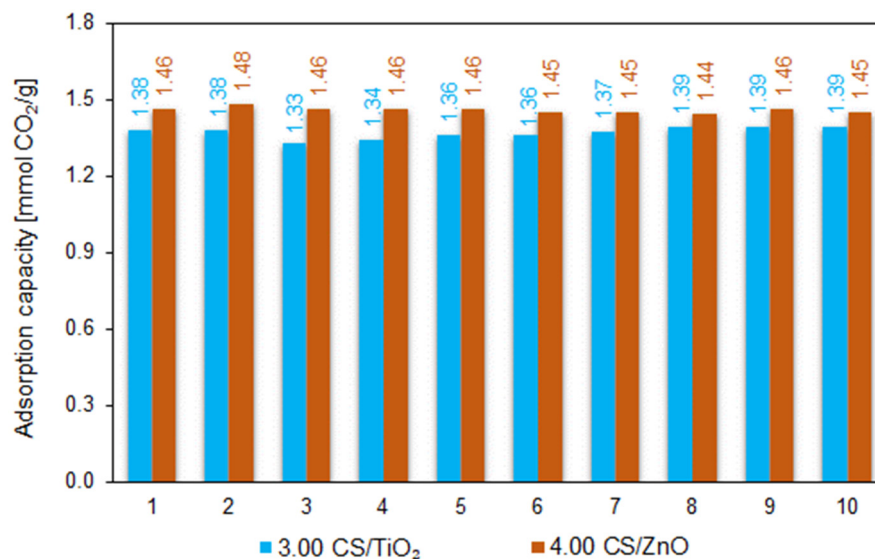


Figure 8. Multicyclic stability of CO₂ adsorption–desorption measured at 30 °C for 4.00 CS/TiO₂ and 3.00 CS/TiO₂ samples.

During ten cycles, the adsorption capacity for both groups of tested samples was similarly constant, without noticeable degradation in the adsorption capacity of CO₂. The average adsorption capacity after 10 consecutive runs reached 1.37 and 1.46 mmol/g for the 3.00 CS/TiO₂ and 4.00 CS/ZnO, respectively. From these results, we can conclude that the carbon spheres exhibited significant CO₂ adsorption capacity and showed excellent stability and regenerability—A crucial criterion for evaluating adsorbents for CO₂ capture applications.

Although, as mentioned before, for the CS/TiO₂ composites with a higher content of carbon the volume of the mesopores decreased, and for the 3.00 CS/TiO₂ sample decreased drastically, the amount of the adsorbed CO₂ increased. It clearly indicates that mesopores did not affect the amount of the adsorbed CO₂, and the observed changes are related to the development of the microporosity of the composites. For this reason, the influence of the carbon concentration on the ultra-microporosity of the obtained composites' pore

size distributions was also studied. The values of the ultra-micropores' volume were calculated based on the CO₂ adsorption at 0 °C (Figure 6) using the NLDFT model, and the results are presented in Figure 9 and Table 1. The overall content of ultra-micropores for the samples with a lower carbon content (0.05 g; 0.1 g; 0.25 g) was similar and did not change significantly with the increased carbon content. Nevertheless, the contribution of 0.35 nm pores and 0.55 nm pores slightly increased. Considerable development of the ultra-microporosity was noticed when the carbon content reached 0.5 g and more. Higher contribution of carbon in the obtained composites caused the development of the pores 0.35 and 0.55 nm in size, reaching a maximum for the 3.00 CS/TiO₂ sample. Hence, the adsorption properties of these samples towards CO₂ have increased. Interestingly, the sample assigned as 1.20 CS/TiO₂ was characterized by a very low content of 0.35 nm pores. However, the second peak starts at about 0.4 nm in size and indicates a broader range of the pores over 0.4 nm.

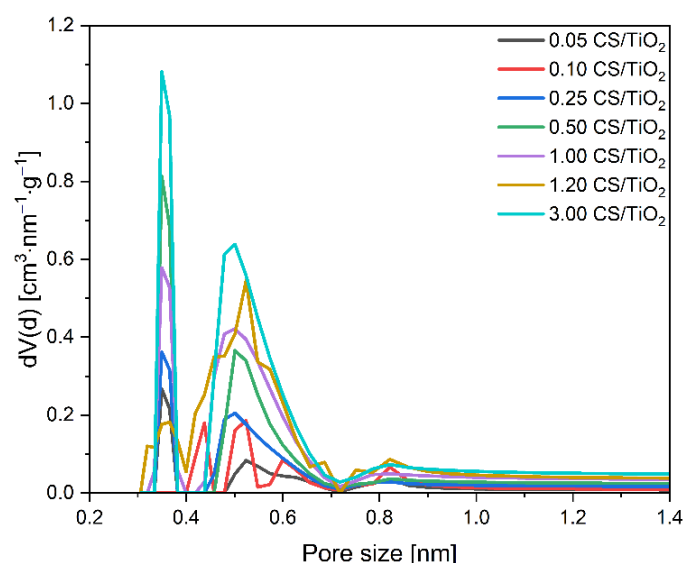


Figure 9. Pore size distributions of the obtained CS/TiO₂ composites.

The same tendency can be noticed considering the CO₂ adsorption on the CS/ZnO composites. It means that, with the increase in carbon content, CO₂ adsorption values increased, reaching a maximum for the 4.00 CS/ZnO sample of 2.70 mmol/g. For this material, the lowest content of mesopores and the highest content of micropores were also observed. The pore size distributions of the CS/ZnO composites were also investigated and are given in Figure 10 and Table 1. Increasing the carbon content, a higher contribution of the 0.35 nm pores and 0.55 nm pores can be noticed in contrast to the 0.10 CS/ZnO sample. It should also be noted that comparing the two types of composites, for the CS/TiO₂ samples with a carbon content up to 1 g, the values of CO₂ adsorption obtained at 0 °C were slightly higher than for CS/ZnO. For example, using a 1.00 CS/TiO₂ sample, 1.75 mmol/g of CO₂ could be adsorbed at 0 °C, but using 1.00 CS ZnO material, only 1.54 mmol/g of CO₂. Similar values were already noticed for the samples with carbon content above 1 g, regardless of the type of oxide present. Simultaneously for the CS/TiO₂ material, a slightly higher content of micropores was noticed. It confirms a significant correlation between efficient CO₂ adsorption at 0 °C and the presence of pores below 0.6 nm.

One important use of molecular models for adsorption is to examine multicomponent adsorption, as this type of adsorption is of obvious importance for practical applications. Adsorption isotherms, shown in Figure 11a,b were measured at a temperature of 25 °C up to a pressure of 1 bar.

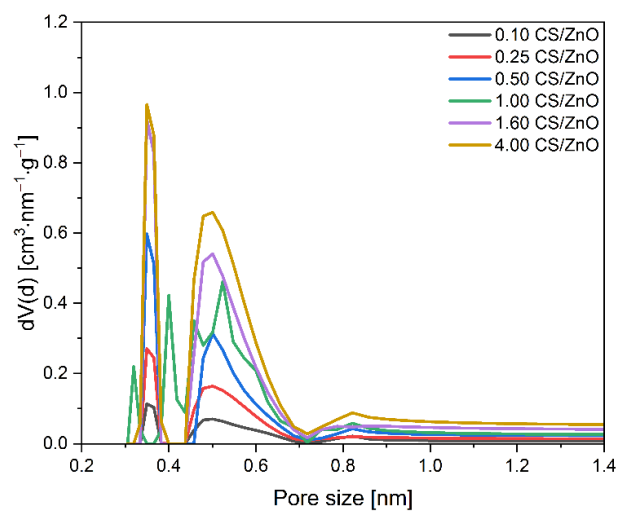


Figure 10. Pore size distributions of the obtained CS/ZnO composites.

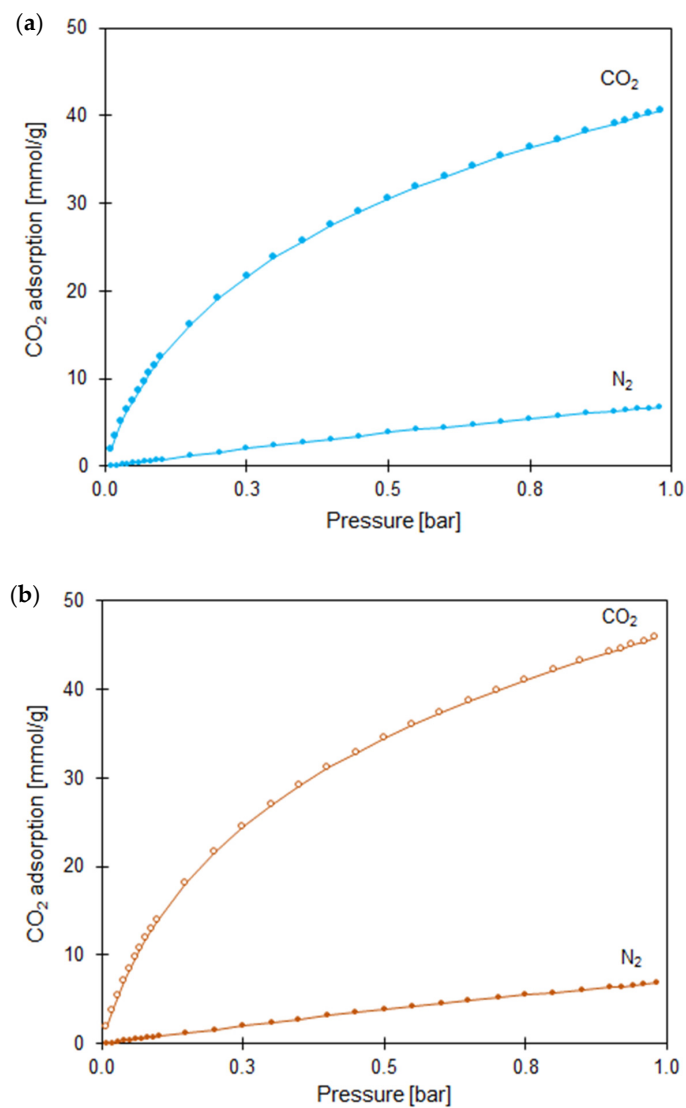


Figure 11. A comparison of single component CO₂ and N₂ adsorption isotherms for (a) 3.00 CS/TiO₂ and (b) 4.00 CS/ZnO samples.

Comparing the adsorption of CO₂ and the adsorption of N₂ for TiO₂- and ZnO-modified CS at the same pressure and temperature conditions, we clearly see that the adsorption of CO₂ (1.66 and 1.88 mmol/g, respectively) was much larger than that of N₂ (0.28 mmol/g) across the entire pressure range, leading to the conclusion that the obtained nanocomposites exhibit good selectivity for CO₂-over-N₂ adsorption. Therefore, the S_{IAST} values calculated according to Equation (2), reached 15.90 and 16.95 for 3.00 CS/TiO₂ and 4.00 CS/ZnO samples, respectively.

The CO₂/N₂ selectivity calculated for two representative samples (3.00 CS/TiO₂ and 4.00 CS/ZnO) is shown in Figure 12. The highest CO₂/N₂ selectivity ratio at 0.1 bar was 49.5 and 61.6, and rapidly decreased with the pressure (up to ~0.3 bar), ultimately reaching values of 5.9 and 9.8 for 3.00 CS/TiO₂ and 4.00 CS/ZnO, respectively, at the pressure around 1 bar. As expected, the selectivity ratio decreased due to the small gas molecules being well absorbed in narrow pores at low pressures. Moreover, CO₂ has a stronger tendency to combine with carbon pores than N₂. Once the adsorption sites are unavailable with pressure increase, the remaining gas molecules are squeezed into the confined pores [55].

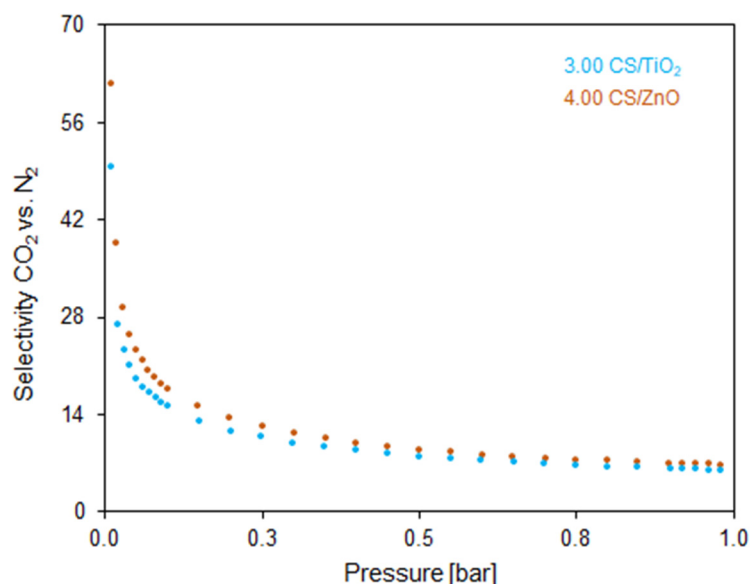


Figure 12. Selectivity of CO₂ over N₂ at 25 °C for 3.00 CS/TiO₂ and 4.00 CS/TiO₂ samples.

3. Materials and Methods

3.1. Materials

Carbon spheres (CS) were obtained from resorcinol and formaldehyde. For this purpose, 2.4 g of resorcinol was dissolved in an aqueous alcohol solution composed of 240 mL distilled water and 96 mL of ethanol. To adjust pH to ~9, ammonium hydroxide (25 wt.%) was slowly dropped into the beaker. Then, 3.6 mL of formaldehyde (37 wt.%) was added, and the whole was mixed using a magnetic stirrer at ambient conditions to facilitate a polycondensation reaction. After 24 h, the mixture was transferred into a microwave reactor (Ertec-Poland, Wrocław, Poland), and the treatment there was carried out for 15 min under a reaction pressure of 20 atm. Next, the products were dried for 24 h at 80 °C and then carbonized in a HST 12/400 Carbolite high-temperature furnace (Carbolite Gero Ltd., Sheffield, UK) under argon atmosphere with the temperature increasing from 20 to 350 °C at a heating rate of 1 °C/min and holding time of 2 h and from 350 to 700 °C at a heating rate of 1 °C/min. After 2 h, the sample was cooled to room temperature under an argon atmosphere. The as-obtained material was washed with distilled water and dried for 48 h at 80 °C in air. The as-prepared carbon spheres in the appropriate amount (from 0.05 to 4 g) were placed into the beaker with 100 mL of ethylene alcohol and stirred for 30 min. Then, 1 g of titanium dioxide (AEROXIDE® TiO₂ P25; Evonik Industries AG, Essen, Germany) or zinc oxide nanopowder (<100 nm particle size; Sigma-Aldrich, St. Louis, MO, USA) was

added, and the whole was stirred again, but this time for 24 h. Afterwards, the obtained mixture was transferred into a microwave-assisted solvothermal reactor (Ertec, Wrocław, Poland), and the treatment there was carried out for 15 min under a reaction pressure of 20 atm. Finally, the obtained composites were dried for 48 h at 80 °C in air.

3.2. Characterization Methods

The chemical structure of tested materials was investigated by the Thermo Scientific Nicolet 380 spectrometer (Thermo Fisher Scientific Inc., Waltham, MA, USA). Samples were prepared by grinding the investigated material with KBr (Merck KGaA, Darmstadt, Germany) and forming pellets. The procedure of pellets' preparation was described in detail in our previous work [30]. For better visualization, all spectra were multiplied by 5.

Thermogravimetric analysis (TG/DTG) was conducted using NETZSCH STA 449 F3 Jupiter (Erich NETZSCH GmbH & Co. Holding KG, Selb, Germany). For this purpose, the sample mass of about 10 mg was placed in an open corundum crucible with a corresponding empty referent pan. Thermal oxidative stability of all samples was measured at a heating rate of 10 °C/min under a flow of air atmosphere (70 mL/min). The analyses were performed over the temperature range of 30–1000 °C.

Surface properties were determined using N₂ adsorption/desorption isotherms performed on a QUADRASORB evo™ Gas Sorption automatic system (Quantachrome Instruments, Boynton Beach, FL, USA) at −196 °C. Before each adsorption experiment, samples were outgassed at 250 °C under a vacuum of 1×10^{-5} mbar for 12 h using a MasterPrep multi-zone flow/vacuum degasser from Quantachrome Instruments to remove adsorbed species that could intervene in the adsorption processes. The surface area (S_{BET}) was determined in the relative pressure range of 0.05–0.3 and calculated based on Brunauer–Emmett–Teller (BET) equation. The total pore volume (TPV) was calculated from the volume of nitrogen held at the highest relative pressure ($p/p_0 = 0.99$). The volume of micropores V_m with diameter below 2 nm was calculated as a result of integrating the pore volume distribution function using the DFT method; the volume of mesopores V_{meso} with diameter from 2 to 50 nm was calculated from the difference in the total pore volume TPV and the volume of micropores V_m .

Carbon dioxide adsorption isotherms at 0 and 25 °C were measured using the same Quadrasorb™ automatic system (Quantachrome Instruments, Boynton Beach, FL, USA) mentioned above in the pressure range between 0.01 and 0.98 bar. From CO₂ adsorption, the isotherms at 0 °C, pore size distribution (PSD), and the volume of ultra-micropores V_s below 1.0 nm (<1 nm) were determined and calculated by integrating the pore volume distribution function using the NLDFT method.

The carbon dioxide cyclic adsorption–desorption measurements were investigated using a thermogravimetric analyzer NETZSCH STA 449 F3 Jupiter. First, the tested samples were pre-dried at 105 °C in pure argon flow (70 mL/min) for 60 min to remove physisorbed moisture and/or CO₂ (from the surface and/or pores), then cooled to the adsorption temperature (30 °C). After the temperature stabilized, the argon flow was reduced to 10 mL/min (used as a protective gas), switched on pure CO₂ and held for 60 min in a flow of 90 mL/min. After adsorption, the gas was switched from CO₂ to argon (70 mL/min), and the temperature increased to 105 °C to desorb the CO₂. The 10 consecutive adsorption–desorption cycles were performed to evaluate the stability of tested adsorbents, and after each adsorption–desorption run, the sample weight was recorded to calculate the CO₂ uptake.

Additionally, to test the selectivity of CO₂ adsorption over N₂ carried out the nitrogen adsorption–desorption measurements at 25 °C up to a pressure of 1 bar, using the Quantachrome Instruments Quadrasorb apparatus, were performed for 3.00 CS/TiO₂ and 4.00 CS/ZnO samples with the best CO₂ adsorption at 0 and 25 °C. To determine the selectivity of the CO₂ and N₂ molecules, we compared the CO₂ and N₂ adsorption from the binary mixture simulations with the CO₂ and N₂ adsorption from the single-component isotherms.

The ideal adsorption solution theory (IAST) was used for the prediction of CO₂/N₂ binary mixture adsorption equilibrium using single components adsorption data according to (Equation (1)):

$$S_{\text{CO}_2} = \frac{q_{\text{CO}_2(p)}}{q_{\text{N}_2(p)}} \quad (1)$$

where: $q_i(p)$ —the adsorption capacity (mmol/g) at the same partial pressure p .

Developed by Myers and Prausnitz [56], the ideal adsorbed solution theory (IAST) is widely used for readily predicting multicomponent adsorption isotherms from only pure-component adsorption isotherms at the same temperature. Carbon dioxide selectivity for a gas mixture containing 85% of N₂ and 15% of CO₂ from 0 to 1 bar was calculated according to Equation (2):

$$S_{0.15:0.85} = \frac{q_{\text{CO}_2 \text{ at } 0.15 \text{ bar}}}{q_{\text{N}_2 \text{ at } 0.85 \text{ bar}}} \times \frac{0.85}{0.15} \quad (2)$$

where: $q_{\text{CO}_2 \text{ at } 0.15 \text{ bar}}$ —the CO₂ uptake (mmol/g) at the partial pressure of 0.15 bar, $q_{\text{N}_2 \text{ at } 0.85 \text{ bar}}$ —the N₂ uptake (mmol/g) at the partial pressure of 0.85 bar.

During the measurements, air, argon, carbon dioxide, and nitrogen gases with a purity of 99.995% (Air Liquide, Białystok-Zaścianki, Poland) were used.

4. Conclusions

The properties of the composites based on carbon spheres and titanium dioxide, or carbon spheres and zinc oxide were compared. The thermal oxidative analysis and FT/IR measurements confirmed the presence of different carbon functional groups in tested samples, mainly unsaturated C=C from amorphous carbon and C–O(H). FT/IR analysis revealed the presence of other groups in the form of C–H. Additionally, the increased spherical carbon content in composites further broadens the combustion temperature range (the oxidative decomposition process starts at a lower temperature). However, the more metal oxide added, the narrower the combustion range. Notably, the detailed structural studies showed that the much higher values of total pore volume for the materials with the addition of titanium dioxide, caused by the higher contribution of mesopores in the samples, did not influence the carbon dioxide adsorption. Simultaneously, in the case of CS/TiO₂ material with the highest carbon content, for which a significant decrease in the volume of mesopores was observed, the decrease in CO₂ adsorption was not noticed. Generally, slightly lower values of CO₂ adsorption were noted for CS/ZnO samples with carbon content up to 1 g than for CS/TiO₂ due to a slightly lower content of micropores for these materials. For the composites with a carbon content above 1 g, the same amount of CO₂ was adsorbed regardless of the type of oxide present in the composite. In both groups of composites, the incorporation of higher carbon content led to the development of ultra-microporosity. It was found that the size of micropores played an essential role, and the pores below 0.6 nm were responsible for efficient CO₂ adsorption. Using the representative 3.00 CS/TiO₂ and 4.00 CS/ZnO samples with the highest adsorption capacity at 0 and 25 °C, it was also found that the synthesized composite materials were characterized by very good stability and regenerability (measured during ten consecutive CO₂ adsorption–desorption cycles). The CO₂/N₂ selectivity checked for the first time for spherical carbon-based composites showed a stronger tendency of CO₂ to combine with carbon pores than N₂.

Author Contributions: Conceptualization: U.N., I.P. and E.K.-N.; Methodology: I.P., P.S. and D.S.; Formal Analysis: I.P., D.S., P.S., E.K.-N., J.K.-K. and A.W.; Investigation: P.S., D.S., K.P., A.M., J.K.-K. and A.W.; Writing—Original Draft Preparation: I.P., E.K.-N., P.S., D.S., F.L., A.W. and J.K.-K.; Writing—Review and Editing, U.N., I.P. and E.K.-N.; Visualization: P.S., D.S., A.W. and J.K.-K.; Supervision: U.N. and A.W.M.; Funding Acquisition: U.N. All authors have read and agreed to the published version of the manuscript.

Funding: The research leading to these results has received funding from the Norway Grants 2014-2021 via the National Centre for Research and Development under the grant number NOR/POLNORCCS/PhotoRed/0007/2019-00.

Institutional Review Board Statement: Not applicable.

Informed Consent Statement: Not applicable.

Data Availability Statement: The data presented in this study will be available upon request.

Conflicts of Interest: The authors declare no conflict of interest.

Sample Availability: Samples of the compounds presented in this paper are available from the authors for fee.

References

1. Intergovernmental Panel on Climate Change. Special Report on Global Warming of 1.5 °C. Available online: https://www.ipcc.ch/site/assets/uploads/sites/2/2019/06/SR15_Full_Report_High_Res.pdf (accessed on 26 June 2022).
2. Our World in Data. Available online: <https://ourworldindata.org/emissions-by-sector> (accessed on 26 June 2022).
3. Sovacool, B. Valuing the greenhouse gas emissions from nuclear power: A critical survey. *Energy Policy* **2008**, *36*, 2950–2963. [[CrossRef](#)]
4. Boot-Handford, M.E.; Abanades, J.C.; Anthony, E.J.; Blunt, M.J.; Brandani, S.; Mac Dowell, N.; Fernández, J.R.; Ferrari, M.-C.; Gross, R.; Hallett, J.P.; et al. Carbon capture and storage update. *Energy Environ. Sci.* **2014**, *7*, 130–189. [[CrossRef](#)]
5. Al-Mamoori, A.; Krishnamurthy, A.; Rownaghi, A.; Rezaei, F. Carbon capture and utilization update. *Energy Technol.* **2017**, *5*, 834–849. [[CrossRef](#)]
6. Kelemen, P.; Benson, S.; Pilorgé, H.; Psarras, P.; Wilcox, J. An overview of the status and challenges of CO₂ storage in minerals and geological formations. *Front. Clim.* **2019**, *1*, 9. [[CrossRef](#)]
7. Zahid, U.; Lim, Y.; Jung, J.; Han, C. CO₂ geological storage: A review on present and future prospects. *Korean J. Chem. Eng.* **2011**, *28*, 674–685. [[CrossRef](#)]
8. Li, L.; Zhao, N.; Wei, W.; Sun, Y. A review of research progress on CO₂ capture, storage, and utilization in Chinese Academy of Sciences. *Fuel* **2013**, *108*, 112–130. [[CrossRef](#)]
9. Osman, A.; Hefny, M.; Abdel Maksoud, M.; Elgarahy, A.; Rooney, D. Recent advances in carbon capture storage and utilisation technologies: A review. *Environ. Chem. Lett.* **2020**, *19*, 797–849. [[CrossRef](#)]
10. Song, C.; Liu, Q.; Deng, S.; Li, H.; Kitamura, Y. Cryogenic-based CO₂ capture technologies: State-of-the-art developments and current challenges. *Renew. Sustain. Energy Rev.* **2019**, *101*, 265–278. [[CrossRef](#)]
11. Dideikin, A.; Vul, A. Graphene oxide and derivatives: The place in graphene family. *Fron. Phys.* **2019**, *6*, 149. [[CrossRef](#)]
12. Sharma, A.; Jindal, J.; Mittal, A.; Kumari, K.; Maken, S.; Kumar, N. Carbon materials as CO₂ adsorbents: A review. *Environ. Chem. Lett.* **2021**, *19*, 875–910. [[CrossRef](#)]
13. Qiao, W.M.; Song, Y.; Lim, S.Y.; Hong, S.H.; Yoon, S.H.; Mochida, I.; Imaoka, T. Carbon nanospheres produced in an arc-discharge process. *Carbon* **2006**, *44*, 187–190. [[CrossRef](#)]
14. Li, M.; Li, W.; Liu, S. Hydrothermal synthesis, characterization, and KOH activation of carbon spheres from glucose. *Carbohydr. Res.* **2011**, *346*, 999–1004. [[CrossRef](#)]
15. Panickar, R.; Sobhan, C.; Chakravorti, S. Chemical vapor deposition synthesis of carbon spheres: Effects of temperature and hydrogen. *Vacuum* **2020**, *172*, 109108. [[CrossRef](#)]
16. Pol, V.G.; Shrestha, L.K.; Ariga, K. Tunable, functional carbon spheres derived from rapid synthesis of resorcinol-formaldehyde resins. *ACS Appl. Mater. Interfaces* **2014**, *6*, 10649–10655. [[CrossRef](#)]
17. Liu, J.; Qiao, S.Z.; Liu, H.; Chen, J.; Orpe, A.; Zhao, D.; Lu, G.X. Extension of the Stöber method to the preparation of monodisperse resorcinol-formaldehyde resin polymer and carbon spheres. *Angew. Chem. Int. Ed.* **2011**, *50*, 5947–5951. [[CrossRef](#)] [[PubMed](#)]
18. Wickramaratne, N.; Jaroniec, M. Activated carbon spheres for CO₂ adsorption. *ACS Appl. Mater. Interfaces* **2013**, *5*, 1849–1855. [[CrossRef](#)]
19. Choma, J.; Kloske, M.; Dziura, A.; Stachurska, K.; Jaroniec, M. Preparation and studies of adsorption properties of microporous carbon spheres. *Environ. Prot. Eng.* **2016**, *19*, 169–182. [[CrossRef](#)]
20. Yue, L.; Xia, Q.; Wang, L.; Wang, L.; DaCosta, H.; Yang, J.; Hu, X. CO₂ adsorption at nitrogen-doped carbons prepared by K₂CO₃ activation of urea-modified coconut shell. *J. Colloid Interface Sci.* **2018**, *511*, 259–267. [[CrossRef](#)]
21. Meng, L.; Park, S. Effect of ZnCl₂ activation on CO₂ adsorption of N-doped nanoporous carbons from polypyrrole. *J. Solid State Chem.* **2014**, *218*, 90–94. [[CrossRef](#)]
22. Wang, Y.; Chang, B.; Guan, D.; Dong, X. Mesoporous activated carbon spheres derived from resorcinol-formaldehyde resin with high performance for supercapacitors. *J. Solid State Electrochem.* **2015**, *19*, 1783–1791. [[CrossRef](#)]
23. Choma, J.; Osuchowski, L.; Marszewski, M.; Dziura, A.; Jaroniec, M. Developing microporosity in Kevlar®-derived carbon fibers by CO₂ activation for CO₂ adsorption. *J. CO₂ Util.* **2016**, *16*, 17–22. [[CrossRef](#)]

24. Zhou, J.; Luo, A.; Zhao, Y. Preparation and characterisation of activated carbon from waste tea by physical activation using steam. *J. Air Waste Manag. Assoc.* **2018**, *68*, 1269–1277. [[CrossRef](#)] [[PubMed](#)]
25. Ludwinowicz, J.; Jaroniec, M. Potassium salt-assisted synthesis of highly microporous carbon spheres for CO₂ adsorption. *Carbon* **2015**, *82*, 297–303. [[CrossRef](#)]
26. Sibera, D.; Narkiewicz, U.; Kapica, J.; Serafin, J.; Michalkiewicz, B.; Wróbel, R.; Morawski, A.W. Preparation and characterisation of carbon spheres for carbon dioxide capture. *J. Porous Mater.* **2018**, *26*, 19–27. [[CrossRef](#)]
27. Kandy, M. Carbon-based photocatalysts for enhanced photocatalytic reduction of CO₂ to solar fuels. *Sustain. Energy Fuels* **2020**, *4*, 469–484. [[CrossRef](#)]
28. Yamamoto, O.; Sawai, J.; Sasamoto, T. Activated carbon sphere with antibacterial characteristics. *Mater. Trans.* **2002**, *43*, 1069–1073. [[CrossRef](#)]
29. Wang, X.; Hu, P.; Fangli, Y.; Yu, L. Preparation and characterization of ZnO hollow spheres and ZnO-carbon composite materials using colloidal carbon spheres as templates. *J. Phys. Chem. C* **2007**, *111*, 6706–6712. [[CrossRef](#)]
30. Pelech, I.; Sibera, D.; Staciwa, P.; Kusiak-Nejman, E.; Kapica-Kozar, J.; Wanag, A.; Narkiewicz, U. ZnO/carbon spheres with excellent regenerability for post-combustion CO₂ capture. *Materials* **2021**, *14*, 6478. [[CrossRef](#)]
31. Pelech, I.; Staciwa, P.; Sibera, D.; Kusiak-Nejman, E.; Morawski, A.W.; Kapica-Kozar, J.; Narkiewicz, U. The effect of the modification of carbon spheres with ZnCl₂ on the adsorption properties towards CO₂. *Molecules* **2022**, *27*, 1387. [[CrossRef](#)]
32. Wang, H.; Wu, Z.; Liu, Y. A simple two-step template approach for preparing carbon-doped mesoporous TiO₂ hollow microspheres. *J. Phys. Chem. C* **2009**, *113*, 13317–13324. [[CrossRef](#)]
33. Bi, T.; Wan, J.; Yang, S.; Yu, X.; Ma, F. Photocatalytic activity of nitrogen-doped mesoporous carbon spheres supporting anatase TiO₂ prepared by a simple two-step solvothermal approach. *Nano* **2015**, *10*, 1550076. [[CrossRef](#)]
34. Morawski, A.; Staciwa, P.; Sibera, D.; Moszyński, D.; Zgrzebnicki, M.; Narkiewicz, U. Nanocomposite titania-carbon spheres as CO₂ and CH₄ sorbents. *ACS Omega* **2020**, *5*, 1966–1973. [[CrossRef](#)]
35. Justh, N.; Bakos, L.P.; Hernádi, K.; Kiss, G.; Réti, B.; Erdélyi, Z.; Parditka, B.; Szilágyi, I.M. Photocatalytic hollow TiO₂ and ZnO nanospheres prepared by atomic layer deposition. *Sci. Rep.* **2017**, *7*, 4337. [[CrossRef](#)]
36. Jayarambabu, N. Germination and growth characteristics of mungbean seeds (*Vigna radiata* L.) affected by synthesized zinc oxide nanoparticles. *Int. J. Curr. Eng. Technol.* **2014**, *4*, 3411–3416.
37. Gordon, S.H.; Mohamed, A.; Harry-O'kuru, R.E.; Imam, S.H. A chemometric method for correcting Fourier transform infrared spectra of biomaterials for interference from water in KBr discs. *Appl. Spectrosc.* **2010**, *64*, 448–457. [[CrossRef](#)] [[PubMed](#)]
38. Deshmukh, A.A.; Mhlanga, S.D.; Coville, N.J. Carbon spheres. *Mater. Sci. Eng. R Rep.* **2010**, *70*, 1–28. [[CrossRef](#)]
39. Farrokhi-Rad, M. Effect of Tris and acetic acid on the stability of titania nanoparticles in different alcohols and their electrophoretic deposition process. *Process. Appl. Ceram.* **2018**, *12*, 56–65. [[CrossRef](#)]
40. Zhang, Q.; Li, J.; Lin, Q.; Fang, C. A stiff ZnO/carbon foam composite with second-level macroporous structure filled ZnO particles for heavy metal ions removal. *Environ. Res.* **2020**, *188*, 109698. [[CrossRef](#)] [[PubMed](#)]
41. Jiang, X.; Yu, L.; Yao, C.; Zhang, F.; Zhang, J.; Li, C. Synthesis and characterization of Gd₂O₃ hollow microspheres using a template-directed method. *Materials* **2016**, *9*, 323. [[CrossRef](#)]
42. Chang, B.; Guan, D.; Tian, Y.; Yang, Z.; Dong, X. Convenient synthesis of porous carbon nanospheres with tunable pore structure and excellent adsorption capacity. *J. Hazard. Mater.* **2013**, *262*, 256–264. [[CrossRef](#)]
43. Demir-Cakan, R.; Baccile, N.; Antonietti, M.; Titirici, M.M. Carboxylate-rich carbonaceous materials via one-step hydrothermal carbonization of glucose in the presence of acrylic acid. *Chem. Mater.* **2009**, *21*, 484–490. [[CrossRef](#)]
44. Wang, G.; Xu, L.; Zhang, J.; Yin, T.; Han, D. Enhanced photocatalytic activity of TiO₂ powders (P25) via calcination treatment. *Int. J. Photoenergy* **2012**, *2012*, 265760. [[CrossRef](#)]
45. Nagaraju, G.; Udayabhanu; Shivaraja; Prashanth, S.A.; Shastri, M.; Yathish, K.V.; Anupama, C.; Rangappa, D. Electrochemical heavy metal detection, photocatalytic, photoluminescence, biodiesel production and antibacterial activities of Ag–ZnO nanomaterial. *Mater. Res. Bull.* **2017**, *94*, 54–63. [[CrossRef](#)]
46. Hongbin, L.; Youzhen, Z.; Sascha, V.; Shaochun, T.; Xiangkang, M. Effects of hydrothermal temperature on formation and decoloration characteristics of anatase TiO₂ nanoparticles. *Sci. China Technol. Sci.* **2012**, *55*, 894–902.
47. Galaburda, M.V.; Bogatyrov, V.M.; Skubiszewska-Zięba, J.; Oranska, O.I.; Sternik, D.; Gun'ko, V.M. Synthesis and structural features of resorcinol-formaldehyde resin chars containing nickel nanoparticles. *Appl. Surf. Sci.* **2016**, *360*, 722–730. [[CrossRef](#)]
48. Lin, C.; Ritter, J.A. Effect of synthesis pH on the structure of carbon xerogels. *Carbon* **1997**, *35*, 1271–1278. [[CrossRef](#)]
49. Sedghi, R.; Asadi, S.; Heidari, B.; Heravi, M.M. TiO₂/polymeric supported silver nanoparticles applied as superior nanocatalyst in reduction reactions. *Mater. Res. Bull.* **2017**, *92*, 65–73. [[CrossRef](#)]
50. Robertson, C.; Mokaya, R. Microporous activated carbon aerogels via a simple subcritical drying route for CO₂ capture and hydrogen storage. *Micropor. Mesopor. Mater.* **2013**, *179*, 151–156. [[CrossRef](#)]
51. Jin, Z.; Gao, C.; Hsu, W.K.; Zhu, Y.; Huczko, A.; Bystrzejewski, M.; Roe, M.; Lee, C.Y.; Acquah, S.; Kroto, H.; et al. Large-scale synthesis and characterization of carbon spheres prepared by direct pyrolysis of hydrocarbons. *Carbon* **2005**, *43*, 1944–1953. [[CrossRef](#)]
52. Thommes, M.; Kaneko, K.; Neimark, A.V.; Olivier, J.P.; Rodríguez-Reinoso, F.; Rouquerol, J.; Sing, K.S. Physisorption of gases, with special reference to the evaluation of surface area and pore size distribution (IUPAC Technical Report). *Pure Appl. Chem.* **2015**, *87*, 1051–1069. [[CrossRef](#)]

53. Guang, Y. Facile one-step synthetic route to mesoporous N-doped attapulgite (ATP)@carbon composite through hydrothermal carbonization and the application to adsorbing toxic metal ions. *Chem. Lett.* **2015**, *44*, 369–371.
54. Ribeiro, E.; Plantard, G.; Teyssandier, F.; Maury, F.; Sadiki, N.; Chaumont, D.; Goetz, V. Activated-carbon/TiO₂ composites preparation: An original grafting by milling approach for solar water treatment applications. *J. Environ. Chem. Eng.* **2020**, *8*, 104115. [[CrossRef](#)]
55. Marsh, H.; Rodríguez Reinoso, F. *Activated Carbon*, 1st ed.; Elsevier Ltd.: Oxford, MS, USA, 2006; pp. 157–164.
56. Myers, A.; Prausnitz, J.M. Thermodynamics of mixed-gas adsorption. *AIChE J.* **1965**, *11*, 121–127. [[CrossRef](#)]